metals

MDPI

Article

Effect of Cooling Rate and Remelting Temperature on the Solidification Structure of Al-5Zr Master Alloy

Zhenhua Li, Wangming Zhang, Siyue Fan * and Qingwei Jiang *

School of Materials Science and Engineering, Kunming University of Science and Technology, Kunming 650500, China

* Correspondence: fansiyue123@sina.com (S.F.); jqw6@163.com (Q.J.)

Abstract: Zr is an important element to improve the heat resistance of aluminum alloys, which is usually added to alloys using the Al-Zr master alloys. The microstructure of Al-Zr master alloys has a significant impact on the properties of Zr-bearing aluminum alloys. In this paper, the microstructure of commercial Al-5Zr master alloys was examined, and the effect of the remelting temperature and cooling rate on the solidification structure of the remelted Al-5Zr master alloys was investigated, aiming to develop a feasible way for quality improvement of Al-5Zr master alloys. The results showed that the microstructure of the remelted Al-5Zr master alloy could be regulated effectively by controlling the remelting temperature and cooling rate. When the remelting temperature was 1320 °C, the primary Al_3Zr phase in the remelted Al-5Zr master alloy was mainly precipitated as coarse plate-like or fine long needle-like. Higher cooling rate increased nucleation density and refined microstructure. The average length of the primary Al_3Zr phase was 178.2, 87.4, and 61.3 µm when the cooling rate was 4.6, 30.8, and 43.9 °C/s, respectively. Lower remelting temperature was generally conducive to refinement of primary Al_3Zr phase. When the remelting temperature was 920 °C, the primary Al_3Zr phase in the remelted Al-5Zr master alloy was mainly precipitated as block-like, fine needle-like, and petal-like. When the cooling rate was 4.6 °C, coarse plate-like Al_3Zr phase precipitated. With increasing cooling rate to 25.3 °C, the coarse plate-like Al_3Zr phase disappeared and the block-like and fine needle-like Al_3Zr phase precipitated followed by a large number of fine petal-like Al_3Zr phase precipitated after cooling rate to 45.6 °C. The optimized remelting process can improve the microstructure of the commercial Al-5Zr master alloy.

Keywords: Al-Zr master alloys; cooling rate; remelting temperature; solidification structure

Citation: Li, Z.; Zhang, W.; Fan, S.; Jiang, Q. Effect of Cooling Rate and Remelting Temperature on the Solidification Structure of Al-5Zr Master Alloy. *Metals* **2023**, *13*, 749. https://doi.org/10.3390/met13040749

Academic Editor: Maciej Motyka

Received: 15 March 2023
Revised: 1 April 2023
Accepted: 10 April 2023
Published: 12 April 2023

1. Introduction

Aluminum alloys, one of the important lightweight materials, have been attracting increasing attention due to their high specific strength, good processing properties, and electrical conductivities [1]. Because of these advantages, aluminum alloys are widely used in aerospace, military fields, as well as transmission line industries [2,3]. Zirconium (Zr) is an effective alloying element to improve the performance of aluminum alloys, especially their heat resistance [4]. Previous studies had proven that the formation of metastable Al_3Zr precipitates with $L1_2$ cubic structure can enhance the aging strengthening ability and thermal stability of aluminum alloys below 400 °C [5,6]. However, coarse primary Al_3Zr particles are easily precipitated in the Zr-bearing aluminum alloys due to the low solubility of Zr in Al (660 °C: 0.28%) and diffusivity (400 °C: 1.2 × 10–20 m^2/s). These primary Al_3Zr particles have a high thermal stability, making them difficult to dissolve during the homogenization process. The formation of primary Al_3Zr will reduce the properties of Zr-bearing aluminum alloys because they reduce the saturation of Zr in Al, thus decreasing the aging strengthening ability of Zr in Al [7–9]. Therefore, it is essential to prevent the formation of coarse primary Al_3Zr in the Zr-bearing aluminum alloys.

It has been demonstrated in the modern research and production practices that there is the "heredity effect" in the production process of cast alloys. As early as the 1920s, there was research on the "heredity effect" in the field of steel [10]. After the confirmation of the "heredity effect", more and more researchers and institutions have shown great interest in the "heredity effect" of non-ferrous metals, especially aluminum and its alloys [11,12]. Recently, many studies have discussed the effect of organization heredity of raw materials on the organization of products. Li et al. [13] reported that the grain size of conventional A356 aluminum alloy ingot was abnormally large, which usually caused shrinkage, uneven organization, and other defects in casting, which was not conducive to the performance of the alloy. They studied the organizational heredity of fine-grained Al-Mg-Si alloy, and the results showed that the fine-grained A356 aluminum alloy had obvious organizational heredity, which was not affected by the insulation time after remelting and heat treatment. Compared with the conventional A356 aluminum alloy, when the fine-grained A356 aluminum alloy was used for remelting, the TCB particles existing in the fine-grained A356 aluminum alloy could survive stably, reducing the undercooling of α-Al grain nuclei, so that the fine-grained organization could be inherited in the casting. Wu et al. [14] studied the organizational heredity of Si phase in the high-purity Al-Si alloy. They reported that the size and shape of eutectic Si in the master alloy prepared by using different purity Si raw materials were different. When the purity of the raw material was higher, the eutectic Si phase in the prepared master alloy was finer and more in number. When the purity of the raw material was lower, the eutectic Si phase in the prepared master alloy was coarse plate-like and large with rough surface. They also found that the size and shape of the eutectic Si in these two master alloys significantly affected the existence form of Si in the prepared Al-1.0%Si alloy, which indicates the existence of Si phase heredity effect in the Al-Si alloy. Sun et al. [15] reported the similar phenomena in the Al-Zr master alloy. The primary Al_3Zr phase has a polycrystalline structure, such as $D0_{23}$ and $L1_2$. Due to the difference of melting conditions, even if the primary Al_3Zr phase is all $D0_{23}$ structure, its shape has obvious differences; and the different shapes of primary phase will have different effects on the casting products, that is, the so-called "heredity effect".

Zr is usually added into the aluminum alloys through the Al-Zr master alloys during casting. The contents of Zr in the Al-Zr master alloy are usually above 3% (mass fraction), and the commonly used Al-5Zr master alloys contain about 5%, which far exceeded the solubility of Zr in the Al liquid. In this case, Zr mainly exists in the form of coarse primary Al_3Zr. Therefore, in order to avoid the adverse effect of the primary phase morphology on the casting product, the morphologies of primary phases should be controlled. Xiang et al. [16] found that through remelting the Al-Si-Mg-Mn alloy under the appropriate melting process and then casting, the morphology of the eutectic phase in the alloy could be effectively improved. After remelting, the alloy has finer eutectic silicon phase and α-phase, and the mechanical properties of the alloy are significantly improved compared with those before remelting due to the improvement in the microstructure. Thus, based on the above discussion, we try to remelt the Al-5Zr master alloy to improve its microstructure in order to reduce the adverse effect of the coarse primary phase on the casting performance.

However, the remelting process parameters need to be explored. This is because the melting temperature and cooling rate have a significant influence on the microstructure of the casting during the casting process. In recent years, some articles have studied the microstructure of Al-5Zr master alloys prepared by flux growth method under different casting processes. Zhu et al. [17] used flux growth method to prepare Al-5Zr master alloy, and reported that increasing cooling rate would be beneficial for size reduction of primary Al_3Zr. Brodova et al. [18] investigated the effect of cooling rate on the morphology of primary Al_3Zr in Al-1.5Zr alloy. With increasing cooling rate from 200 to 20,000 K/s, the morphology of primary Al_3Zr changed from coarse needle-like to fine rose-like. On the other hand, melting temperature is a key factor affecting the nucleation and growth of primary Al_3Zr. Several studies on the Al-Zr master alloys prepared by flux growth method have proven that melting temperature has strong influence on the morphology of primary Al_3Zr [19,20]. These studies provide a reference for the microstructure control of Al-Zr master alloy. Therefore, in order to improve the morphology of the primary phase in the

Al-Zr master alloy by remelting process, the remelting temperature and cooling rate should be taken into consideration.

In this study, the commercial Al-5Zr master alloy was chosen as the experimental object. Based on the examination of the microstructure of the commercial Al-5Zr master alloy, the suitable remelting process was explored to improve its microstructure. The effect of remelting temperature and cooling rate on the morphology of primary Al_3Zr was investigated and the remelting process parameters for improving microstructure of commercial Al-5Zr master alloy were investigated, aiming at refining the microstructure of the commercial Al-5Zr master alloy.

2. Materials and Methods

The experimental material is the commercial Al-5Zr master alloy. The chemical composition of experimental material is listed in Table 1.

Table 1. Chemical composition of Al-5Zr master alloy used in the experiment.

Elements	Zr	Fe	Si	Al
Chemical compositions (wt.%)	4.97	0.2	0.16	Bal.

The Al-5Zr master alloy was remelted in a graphite crucible inside a medium-frequency induction furnace (LiHua Induction Equipment Limited, Dongguan, China), and the remelting temperature was monitored in real-time using an infrared detection device. The Al-5Zr master alloy was heated to the set remelting temperature until the master alloy melts. After the master alloy melts completely, it was allowed to stand for 5 min and the floating slag was removed from the molten surface, and then poured into iron molds with different wall thicknesses to control the cooling rate (low, intermediate, and high). K-type thermocouples were placed in the middle of the molds to measure their corresponding cooling rates. In order to better explore the effect of remelting temperature on the microstructure of remelted Al-5Zr alloy, the remelting temperature was set to 920 °C and 1320 °C, respectively, one higher than the liquidus line and one lower than the liquidus line. According to the Al-Zr phase diagram, casting above the liquidus line, there is only one liquid phase in the melt; while casting below the liquidus line, there is a two-phase region of liquid phase and Al_3Zr phase in the melt.

Test samples were cut around thermocouple, and the optical microscope (OM, Carl Zeiss microscopy GmbH company, Oberkochen, Germany) and scanning electron microscope (SEM, Hitachi Limited, Tokyo, Japan) equipped with energy dispersive spectrometer (EDS, Oxford Instruments, Oxford, United Kingdom) were used to analyze the solidification structure of the remelted Al-5Zr master alloy. Image Pro Plus image analysis software was used to quantify the number and size of the primary Al_3Zr phases in order to investigate the effects of different remelting processes on the primary Al_3Zr phases. Additionally, the average size of grains of the remelted Al-5Zr master alloy was counted using the Image Pro Plus image analysis software. Prior to the OM observation, the metallographic samples were mechanically polished to the mirror surface finish, and subsequently electrolytically polished to make the grain structure visible. The OM samples were electropolished in 92% ethanol and 8% perchloric acid (mass fraction) at 25 V for 12 s. The equilibrium phase diagram of the Al-xZr (wt.%) alloy system was obtained from Thermo-Calc software (Thermo-Calc Software AB company, Stockholm, Sweden) using Aluminum Demo Database (Company, City, State. Country).

3. Results and Discussion

3.1. Microstructure of Al-5Zr Master Alloy

Figure 1 shows the optical micrograph and backscattered electron images of the un-remelted Al-5Zr master alloy. The grain structure of the un-remelted Al-5Zr master alloy consists of the coarse equiaxed grains and the average size of grain is 171.1 μm (Figure 1a).

Additionally, several hole defects can be observed. According to the results of the SEM image, the microstructure of the un-remelted Al-5Zr master alloy is composed of the α-Al matrix and the white second phases are distributed irregularly. It can be seen that the coarse plate-like, coarse block-like, and fine needle-like white second phases are unevenly distributed throughout the α-Al matrix. Figure 2 shows the typical EDS results of the white second phase. The results show that these white second phases are enriched with Al and Zr elements, with an atomic ratio of Al to Zr close to 3:1, which can be identified as Al_3Zr phase. Evidently, the primary Al_3Zr phases formed in the un-remelted Al-5Zr master alloy are relatively coarse with an uneven distribution.

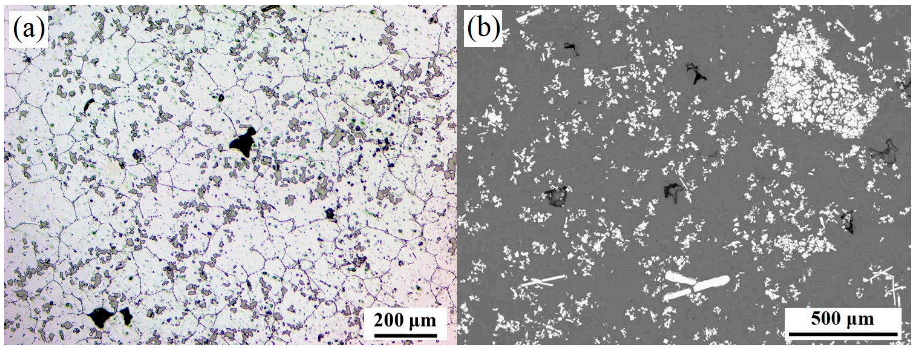

Figure 1. Microstructure of un-remelted Al-5Zr master alloy: (**a**) OM and (**b**) SEM images.

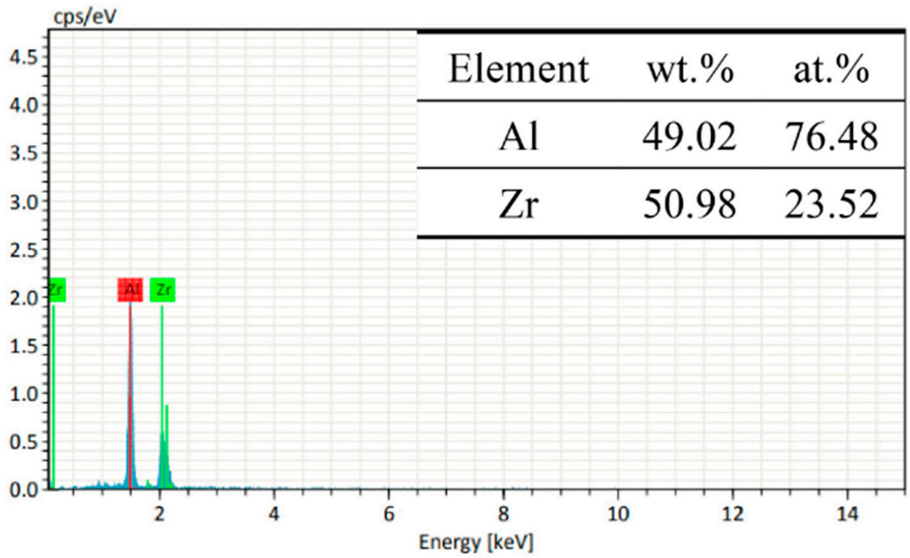

Figure 2. EDS spectrum of the white second phase.

3.2. Cooling Curves at Different Remelting Processes

Figure 3 shows the cooling curves of remelted Al-5Zr master alloy with different cooling rates at different remelting temperatures. The average cooling rates from the casting temperature to 500 °C are marked respectively. It can be seen that the temperature of liquid Al rapidly decreased after casting, regardless of the remelting temperature of 920 °C or 1320 °C, and the cooling rate significantly slows down when the temperature is dropped to 660 °C, as shown in Figure 3. When the temperature decreases near 660 °C, a temperature platform can be observed in the curve of intermediate and low cooling rate. This is the solidus temperature according to the Al-Zr binary phase diagram (Figure 4). However, the temperature platform is not obvious when the cooling rate is high (>25 °C/s).

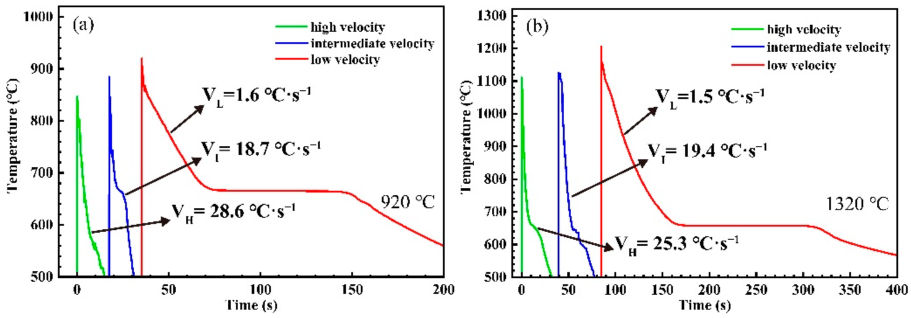

Figure 3. Cooling curves at the different remelting conditions: (**a**) remelting temperature of 920 °C; (**b**) remelting temperature of 1320 °C.

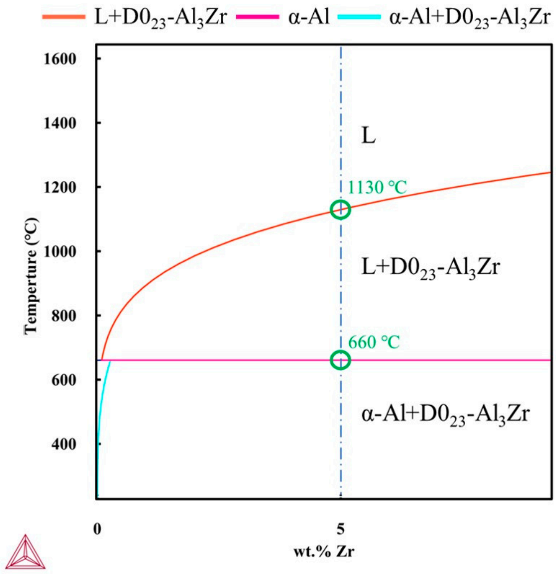

Figure 4. Phase diagram of Al-xZr alloy.

According to the Al-Zr binary phase diagram, the formation temperature range of primary Al_3Zr in the Al-5Zr alloy is considered to be 1130 to 660 °C. It can be found that the cooling rates are different in the formation temperature range of primary Al_3Zr for different remelting processes. When the remelting temperature is 920 °C, the cooling rates in the two-phase region corresponding to low, intermediate, and high velocity are 4.6 °C/s, 25.3 °C/s, and 45.6 °C/s, respectively. When the remelting temperature is 1320 °C, the cooling rates in the two-phase region corresponding to low, intermediate, and high velocity are 4.6 °C/s, 30.8 °C/s, and 43.9 °C/s, respectively.

3.3. The Effect of Remelting Temperature and Cooling Rate on the Grain Structure

Figure 5 shows the grain structure of the remelted Al-5Zr master alloy at different remelting conditions. It can be observed that the grain structures of all remelted Al-5Zr master alloys at different remelting conditions consist of equiaxed grains with different sizes. During solidification, the $D0_{23}$-Al_3Zr will pre-precipitate before the α-Al (Figure 4). Previous studies have confirmed that the $D0_{23}$-Al_3Zr is the effective nucleation nuclei of α-Al. The $D0_{23}$-Al_3Zr has the lattice parameter of a = 0.4013 nm and c = 1.732 nm, and α-Al has the lattice parameter of a = 0.4049 nm [21,22]. Therefore, the $D0_{23}$-Al_3Zr and α-Al have very similar crystal structures and lattice parameters, meaning a small lattice mismatch between these two phases. According to the "principle of coherent interface correspondence", the $D0_{23}$-Al_3Zr is the effective nucleation nuclei of α-Al, promoting the formation of equiaxed grains [23]. The average sizes of grains were counted using the Image Pro Plus image analysis software. The average sizes of grains are 252.9, 56.6, and 47.1 μm, respectively when the remelting temperature is 920 °C, and that are 330.7, 78.9, and 41.2 μm when the remelting temperature is 1320 °C. The results show that the grain structures are gradually refined with the increase in the cooling rates regardless of the remelting temperature is 920 °C or 1320 °C.

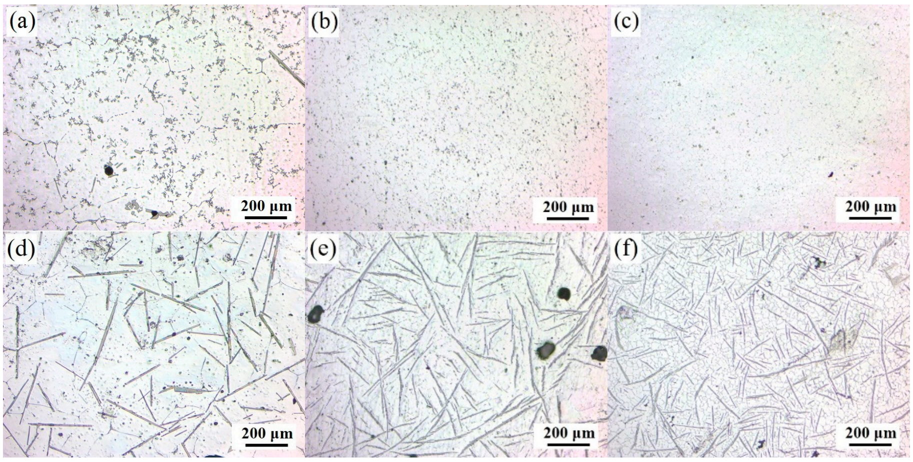

Figure 5. OM images of remelted Al-5Zr master alloy at different remelting conditions: (**a**) cooling rate of 1.6 °C/s, (**b**) cooling rate of 18.7 °C/s, (**c**) cooling rate of 28.6 °C/s, (**a**–**c**) remelting temperature of 920 °C, (**d**) cooling rate of 1.5 °C/s, (**e**) cooling rate of 19.4 °C/s, (**f**) cooling rate of 25.3 °C/s, and (**d**–**f**) remelting temperature of 1320 °C.

3.4. The Effect of Remelting Temperature and Cooling Rate on the Precipitation of Al_3Zr Phase

Figure 6 shows the backscattered electron images and the distribution of Al_3Zr particle lengths in the remelted Al-5Zr master alloy at different cooling rate conditions with a remelting temperature of 920 °C. The statistical results are listed in Figure 6, respectively. The microstructure of the remelted Al-5Zr master alloy mainly consists of the α-Al matrix and a large number of white Al_3Zr phases. When the cooling rate is 4.6 °C/s, a small amount of coarse plate-like and a large amount of fine needle-like or small blocky-like Al_3Zr phases are unevenly precipitated. In this case, although the average length of the long axis of Al_3Zr is only 13.7 μm, the coarse plate-like Al_3Zr with a long axis size over 500 μm is also observed. This indicates that a low cooling rate is not conducive to the refinement of primary Al_3Zr when the remelting temperature is 920 °C. This is because coarse plate-like Al_3Zr will precipitate in this remelting condition. When the cooling rate increases to 25.3 °C/s, the coarse plate-like Al_3Zr disappears and the morphology of Al_3Zr is mainly presented as a mixture of blocky-like and fine needle-like. The segregation of Zr is weakened and the average length of the long axis of Al_3Zr is 15.7 μm. When the cooling rate is 45.6 °C/s, the coarse blocky-like Al_3Zr disappears and a large number of fine petal-like Al_3Zr is precipitated. The average length of the long axis of Al_3Zr is decreased to 11.1 μm. The result demonstrates that the distribution of Al_3Zr is gradually homogenous with the increased cooling rate. When the remelting temperature is 920 °C, the increased cooling rate is conducive to the refinement of primary Al_3Zr.

The liquidus temperature of Al-5Zr alloy is 1130 °C, as shown in Figure 4. When the remelting temperature is 920 °C, there is a two-phase region (L + Al_3Zr). In this case, a large number of Al_3Zr nuclei exist in the melt before casting. When the cooling rate is low (4.6 °C/s), the two-phase region has a long duration, allowing these Al_3Zr nuclei to grow into coarse plate-like, as shown in Figure 6a. When the cooling rate is increased to 25.3 °C/s, the duration of the two-phase region is decreased and these Al_3Zr nuclei grow into blocky-like due to insufficient growth time, resulting in the disappearance of the coarse plate-like Al_3Zr, as shown in Figure 6b. When the highest cooling rate is 45.6 °C/s, the growth of these Al_3Zr nuclei is hindered and the precipitated Al_3Zr has a small average size and a homogenous distribution after solidification, as shown in Figure 6c.

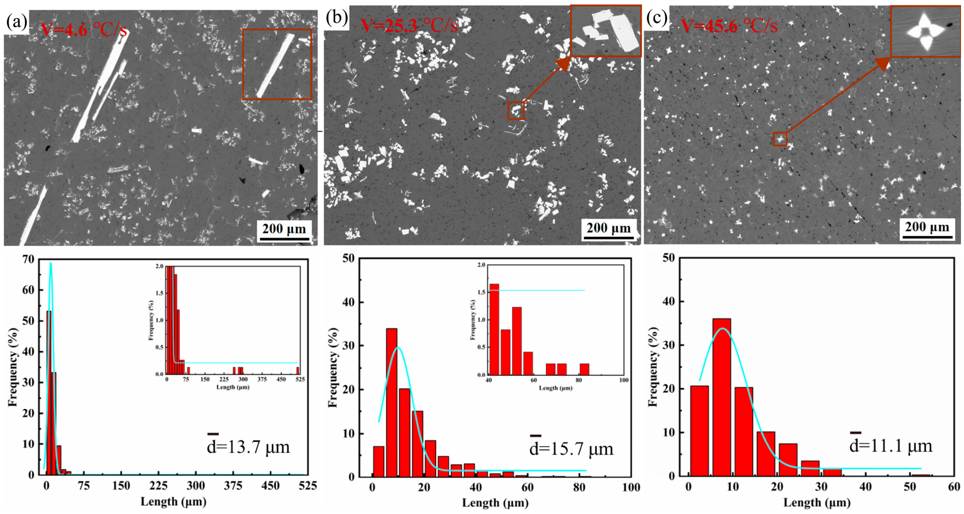

Figure 6. SEM (backscatter electron mode) images and distribution of Al_3Zr particle lengths in the remelted Al-5Zr alloy at different cooling rate conditions with 920 °C remelting temperature (the blue line is the fit curve): (**a**) low velocity; (**b**) intermediate velocity; (**c**) high velocity.

Figure 7 shows the SEM results and distribution of Al_3Zr along the length direction in the remelted Al-5Zr alloy at different cooling rate conditions with a remelting temperature of 1320 °C. It can be observed that the morphology of Al_3Zr precipitated in this case is very different from that of the Al_3Zr precipitated with a remelting temperature of 920 °C. When the remelting temperature is 1320 °C, the morphology of the Al_3Zr precipitated is long needle-like at different cooling rates, as shown in Figure 7a,c. The growth rate of the primary Al_3Zr at different cooling rates can be estimated using the cooling time in the solid-liquid phase region. The results are listed in Table 2.

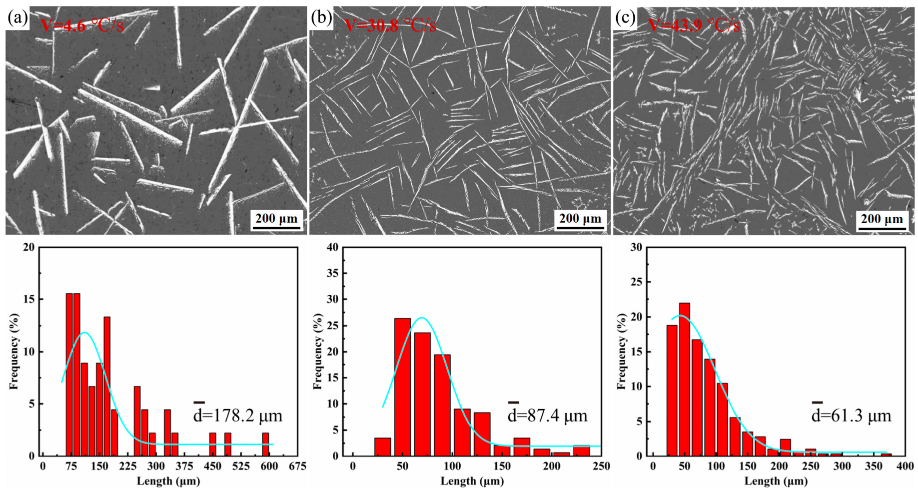

Figure 7. SEM (backscatter electron mode) images and distribution of Al_3Zr particle lengths in the remelted Al-5Zr alloy at different cooling rate conditions with 1320 °C remelting temperature (the blue line is the fit curve): (**a**) low velocity; (**b**) intermediate velocity; (**c**) high velocity.

The results from Figure 7 and Table 2 show that the size and number of long needle-like Al_3Zr are greatly affected by the cooling rate when the remelting temperature is 1320 °C. When the cooling rate is 4.6 °C/s, the morphology of the primary Al_3Zr is coarse plate-like with a long long-axis and wide short-axis. The maximum long-axis length of Al_3Zr is 599.5 μm, the average length of the long-axis is 178.2 μm, and the nucleation density of Al3Zr can be estimated as 44 mm^{-2}. When the cooling rates are 30.8 °C/s and 43.9 °C/s, the morphology of the primary Al_3Zr is the coarse plate-like with a long long-axis and thin short-axis. When the cooling rate is 30.8 °C/s, the average length of the long-axis is

87.4 μm, and the nucleation density of Al_3Zr can be estimated as 119 mm^{-2}. When the cooling rate is 43.9 °C/s, the average length of the long-axis is 61.3 μm, and the nucleation density of Al_3Zr can be estimated as 238 mm^{-2}. The results demonstrate that the number of Al_3Zr increases and the size decreases gradually with increasing cooling rate when the remelting temperature is 1320 °C.

Table 2. Nucleation density and growth rate of Al_3Zr phases during solidifications at 1320 °C.

Cooling Rate (°C·s^{-1})	Holding Time in Two Phase Regions (s)	Largest Long-Axis Length of Al_3Zr (μm)	Nucleation Density (mm^{-2})	Growth Rate along the Long Axis (μm·s^{-1})
4.6	103.2	599.5	44	5.8
30.8	15.3	239.1	119	15.6
43.9	10.9	374.2	238	34.3

When the remelting temperature is higher than the liquidus line, the morphology and size of the primary Al_3Zr precipitates are significantly different from those of the primary Al_3Zr precipitates when the remelting temperature is lower than the liquidus line. This is because almost all of the primary Al_3Zr in the melt at low temperature is dissolved in the Al liquid when the remelting temperature is 1320 °C. In this case, the number of Al_3Zr nuclei is small and the Al_3Zr crystals have enough space for growth after casting. Therefore, the primary Al_3Zr precipitates during solidification and grows into long needle-like [15]. When the cooling rate is 4.6 °C/s, the morphology of primary Al_3Zr is coarse plate-like with a long long-axis and wide short-axis; however, when the cooling rate is relatively large (>30.8 °C/s), the morphology is long needle-like with a long long-axis and thin short-axis. This difference is mainly due to the different growth conditions of Al_3Zr at different cooling rates. When the cooling rate is low, the holding time in the two phase region is long, so Al_3Zr has enough time to grow and the adjacent Al_3Zr stops growing after meeting each other during solidification. However, due to unfinished solidification, Zr atoms will continue to diffuse to the growing Al_3Zr, which makes the short-axis of Al_3Zr wider because the growth in the long-axis direction is hindered. When the cooling rate increases, the larger undercooling will cause the nucleation nuclei in the melt to increase and the number of primary Al_3Zr crystals in the melt will also increase accordingly [24]. However, due to the reduction in holding time in the two-phase region, the growth time of Al_3Zr is shortened, thus the number of Al_3Zr increases and the size decreases gradually with the increase in cooling rate when the remelting temperature is 1320 °C. It should be noted that when the cooling rate is 43.9 °C/s, the largest long-axis length of Al_3Zr is 374.2 μm, while when cooling rate is 30.8 °C/s, the largest long-axis length of Al_3Zr is 239.1 μm. The results indicate that the size of Al_3Zr precipitated is mainly determined by the availability of growth space when the cooling rate is high. Thus, the nucleation density and nucleation position of Al_3Zr crystals become the main factors affecting the morphology and size of the primary Al_3Zr in this case.

In summary, compared with cooling rate, the remelting temperature plays a dominant role in the microstructure of the remelted Al-5Zr master alloy. When the remelting temperature is higher than the liquidus line, the primary phases are the long needle-like and their number increases while the size decreases with the increase in cooling rate. However, when the remelting temperature is below the liquidus line, even with a slow cooling rate, the average size of the primary phases is relatively small due to the existence of pre-existing nuclei in the melt. Nevertheless, when the cooling rate is very slow, even with a remelting temperature lower than the liquidus line, the presence of coarse plate-like primary phases can still be observed. Therefore, remelting at a temperature lower than the liquidus line and cooling at a faster rate (greater than 25.3 °C/s) can significantly improve the microstructure of Al-5Zr master alloy.

4. Conclusions

In this paper, Al-5Zr master alloys were remelted at various conditions, and the microstructure of the remelted alloys were investigated. The conclusions are as follows:

(1) By controlling the remelting temperature and increasing the cooling rate, the morphology, size, and distribution of the primary Al_3Zr in the remelted Al-5Zr master alloy can be further improved.

(2) When the remelting temperature is 920 °C, the morphologies of primary Al_3Zr mainly consist of coarse plate-like, blocky-like, fine needle-like, and petal-like, depending on the cooling rate. When the cooling rate is low (4.6 °C/s), the coarse plate-like Al_3Zr with a long axis size of over 500 μm precipitates, indicating that a low cooling rate is not conducive to the refinement of primary Al_3Zr at 920 °C remelting temperature condition.

(3) When the remelting temperature is 1320 °C, the primary Al_3Zr mainly presents the coarse plate-like and long needle-like at different cooling rates, and increasing the cooling rate is beneficial for the refinement of primary Al_3Zr. When the cooling rate is high (>30.8 °C/s), the nucleation density and nucleation position of Al_3Zr crystals become the main factors affecting the morphology and size of primary Al_3Zr.

Author Contributions: Conceptualization, Z.L., S.F. and Q.J.; methodology, Z.L., S.F. and Q.J.; formal analysis, Z.L., W.Z. and S.F.; investigation, Z.L. and Q.J.; data curation, Z.L., W.Z. and S.F.; writing—original draft preparation, Z.L.; writing—review and editing, Z.L., W.Z., S.F. and Q.J.; project administration, Z.L.; funding acquisition, Z.L. All authors have read and agreed to the published version of the manuscript.

Funding: This research was funded by Key Project of Research and Development Yunnan Province, grant number 202103AN080001-002, 202202AG050007-4 and Key Project of Yunnan Fundamental Research, grant number 202101AS070017.

Data Availability Statement: Further additional data may be obtained by request to the corresponding author.

Acknowledgments: We are very grateful to Kunming University of Science and Technology and Yunnan Innovation Institute of Beihang University for their support of this experiment.

Conflicts of Interest: The authors declare no conflict of interest.

References

1. Liu, Q.; Fan, G.; Tan, Z.; Li, Z.; Zhang, D.; Wang, J.; Zhang, H. Precipitation of Al_3Zr by two-step homogenization and its effect on the recrystallization and mechanical property in 2195 Al–Cu–Li alloys. *Mater. Sci. Eng. A* **2021**, *821*, 141637. [CrossRef]
2. Williams, J.C.; Starke, E.A., Jr. Progress in structural materials for aerospace systems. *Acta Mater.* **2003**, *51*, 5775–5799. [CrossRef]
3. Belov, N.; Alabin, A.; Matveeva, I.; Eskin, D. Effect of Zr additions and annealing temperature on electrical conductivity and hardness of hot rolled Al sheets. *T. Nonferr. Metal Soc. China* **2015**, *25*, 2817–2826. [CrossRef]
4. Li, J.; Zhang, Y.; Li, M.; Hu, Y.; Zeng, Q.; Zhang, P. Effect of combined addition of Zr, Ti and Y on microstructure and tensile properties of an Al-Zn-Mg-Cu alloy. *Mater. Des.* **2022**, *223*, 111129. [CrossRef]
5. Zhang, J.; Chen, Z.; Wang, H. Quasi in-situ analysis of compressive creep behaviors and microstructure evolutions in Al–Zr alloys with Sc and Er additions. *Mater. Sci. Eng. A* **2022**, *852*, 143650. [CrossRef]
6. Jung, J.-G.; Cho, Y.-H.; Kim, S.-D.; Kim, S.-B.; Lee, S.-H.; Song, K.; Euh, K.; Lee, J.-M. Mechanism of ultrasound-induced microstructure modification in Al–Zr alloys. *Acta Mater.* **2020**, *199*, 73–84. [CrossRef]
7. Pan, S.; Qian, F.; Li, C.; Wang, Z.; Li, Y. Synergistic strengthening by nano-sized α-Al(Mn,Fe)Si and Al_3Zr dispersoids in a heat-resistant Al–Mn–Fe–Si–Zr alloy. *Mater. Sci. Eng. A* **2021**, *819*, 141460. [CrossRef]
8. Mohammadi, A.; Enikeev, N.A.; Murashkin, M.Y.; Arita, M.; Edalati, K. Developing age-hardenable Al-Zr alloy by ultra-severe plastic deformation: Significance of supersaturation, segregation and precipitation on hardening and electrical conductivity. *Acta Mater.* **2020**, *203*, 116503. [CrossRef]
9. Kong, Y.; Pu, Q.; Jia, Z.; Liu, M.; Roven, H.J.; Jia, J.; Liu, Q. Microstructure and property evolution of Al-0.4Fe-0.15Zr-0.25Er alloy processed by high pressure torsion. *J. Alloys Compd.* **2020**, *824*, 153949. [CrossRef]
10. Levi, A. Heredity in Cast Iron. *Iron Age* **1927**, *6*, 960.
11. Zhang, Z.; Bian, X.; Wang, Z.; Liu, X.; Wang, Y. Microstructures and grain refinement performance of rapidly solidified Al–Ti–C master alloys. *J. Alloys Compd.* **2002**, *339*, 180–188. [CrossRef]
12. Yu, L.; Liu, X. The relationship between viscosity and refinement efficiency of pure aluminum by Al–Ti–B refiner. *J. Alloys Compd.* **2006**, *425*, 245–250. [CrossRef]

13. Li, D.X.; Han, M.X.; Zhang, J.; Peng, Y.J.; Sun, Q.Q.; Liu, G.L.; Liu, X.F. Microstructure heredity and high yield strength design of fine grained Al-Si-Mg alloys. *Mater. Rep.* **2021**, *35*, 9003–9008.
14. Wu, Y.L.; Hong, T.; Yang, Q.; Nu, L.G. Structure heredity of high purity Al-Si alloys. *Hot Work. Technol.* **2011**, *40*, 65–66.
15. Sun, Y.; Pan, Q.; Luo, Y.; Liu, Y.; Sun, Y.; Long, L.; Li, M.; Wang, X.; Liu, S. Study on the primary Al3Sc phase and the structure heredity of Al-Zn-Mg-Cu-Sc-Zr alloy. *Mater. Charact.* **2020**, *169*, 110601. [CrossRef]
16. Xiangfa, L.; Xiufang, B.; Xiaogang, Q.; Jiaji, M. The heredity of Al-Si-Mg-Mn before and after remelting. *JOM-US* **1997**, *49*, 40–41. [CrossRef]
17. Zhu, Q.F.; Li, F.; Wang, J.; Wang, Q.H.; Wang, W.J.; Cui, J.Z. Effects of cooling rate on solidification structure of Al-5Zr master alloys. *Chin. J. Nonferrous Met.* **2017**, *27*, 8–14.
18. Brodova, I.G.; Bashlykov, D.V.; Manukhin, A.B.; Stolyarov, V.V.; Soshnikova, E.P. Formation of nanostructure in rapidly solidified Al-Zr alloy by severe plastic deformation. *Scr. Mater.* **2001**, *44*, 1761–1764. [CrossRef]
19. Li, F.; Zhu, Q.F.; Li, L.; Zhang, J.; Shao, B.; Cui, J.Z. Effect of pouring temperature on the primary Al_3Zr phase in Al-5Zr master alloy. *Rare Metal Mat. Eng.* **2015**, *44*, 2029–2033.
20. Li, F.; Zhu, Q.F.; Li, L.; Cui, J.Z. Effect of process parameters on primary Al_3Zr phase in Al-Zr master alloys. *J. Northeast. Univ.* **2013**, *34*, 1739–1742+1791.
21. Zheng, Q.; Yang, C.; Wang, S.; Yu, A.; Chen, H.; He, Y. Effect of compound inoculants Ti and Zr on as cast microstructure and mechanical properties of Al–Cu alloy. *Mater. Res. Innov.* **2014**, *18*, S2-59. [CrossRef]
22. Liu, X.; Liu, Y.; Zhou, Z.; Wang, K.; Zhan, Q.; Xiao, X. Grain refinement and crack inhibition of selective laser melted AA2024 aluminum alloy via inoculation with TiC-TiH_2. *Mater. Sci. Eng. A.* **2021**, *813*, 141171. [CrossRef]
23. Guo, X.M.; Yang, C.G.; Qian, B.N.; Xu, Q.; Zhang, H.Y. Effects of inoculants Ti and Zr on the microstructure and properties of 2219 Al-Cu alloy welds. *Acta Metall. Sin.* **2005**, *41*, 397–407.
24. Yi, K.K.; Jiang, F.; Xu, P.; Peng, Y.Y. Growth mechanism of Al_3Zr phase in Al-$_4$Zr alloy. *J. Rare Metals* **2019**, *43*, 213–218.